



Rotational and vibrational temperatures in a hydrogen discharge with a magnetic X-point

著者	Tsankov Tsanko V., Toko Kaoru, Czarnetzki Uwe
journal or publication title	Physics of plasmas
volume	19
number	12
page range	123503
year	2012-12
権利	(C) 2012 American Institute of Physics This article may be downloaded for personal use only. Any other use requires prior permission of the author and the American Institute of Physics. The following article appeared in Phys. Plasmas 19, 123503 and may be found at http://pop.aip.org/resource/1/phpaen/v19/i12/p123503_s1 .
URL	http://hdl.handle.net/2241/118292

doi: 10.1063/1.4769853

Rotational and vibrational temperatures in a hydrogen discharge with a magnetic X-point

Tsanko V. Tsankov, Kaoru Toko, and Uwe Czarnetzki

Citation: *Phys. Plasmas* **19**, 123503 (2012); doi: 10.1063/1.4769853

View online: <http://dx.doi.org/10.1063/1.4769853>

View Table of Contents: <http://pop.aip.org/resource/1/PHPAEN/v19/i12>

Published by the [American Institute of Physics](#).

Related Articles

Controlling output pulse and prepulse in a resonant microwave pulse compressor
J. Appl. Phys. **113**, 054503 (2013)

“Water window” sources: Selection based on the interplay of spectral properties and multilayer reflection bandwidth
Appl. Phys. Lett. **102**, 041117 (2013)

Plasma electron source for the generation of wide-aperture pulsed beam at forevacuum pressures
Rev. Sci. Instrum. **84**, 023301 (2013)

Emittance of positron beams produced in intense laser plasma interaction
Phys. Plasmas **20**, 013111 (2013)

Multifunctional bulk plasma source based on discharge with electron injection
Rev. Sci. Instrum. **84**, 013307 (2013)

Additional information on Phys. Plasmas

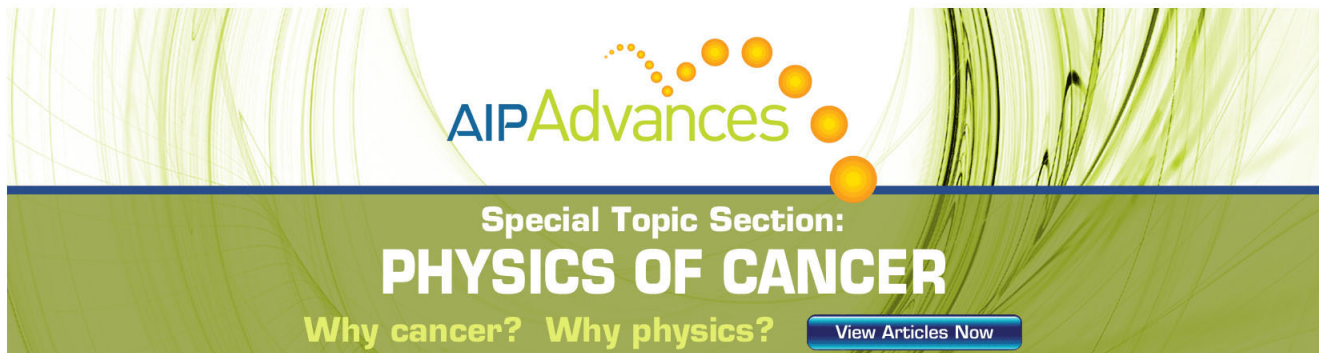
Journal Homepage: <http://pop.aip.org/>

Journal Information: http://pop.aip.org/about/about_the_journal

Top downloads: http://pop.aip.org/features/most_downloaded

Information for Authors: <http://pop.aip.org/authors>

ADVERTISEMENT



AIP Advances

Special Topic Section:
PHYSICS OF CANCER

Why cancer? Why physics? [View Articles Now](#)

Rotational and vibrational temperatures in a hydrogen discharge with a magnetic X-point

Tsanko V. Tsankov,^{1,a)} Kaoru Toko,² and Uwe Czarnetzki¹

¹*Institute for Plasma and Atomic Physics, Ruhr University Bochum, 44780 Bochum, Germany*

²*Institute of Applied Physics, University of Tsukuba, Tsukuba, Ibaraki 305-8573, Japan*

(Received 19 July 2012; accepted 20 November 2012; published online 7 December 2012)

A novel plasma source with a magnetic X-point has been developed to probe an alternative for cesium-free negative hydrogen ion production. This study presents first results for the gas and vibrational temperatures in the source at 1 Pa and various RF powers. The temperatures are obtained from analysis of the intensity distribution of the molecular Fulcher- α bands. The gas temperature increases with the RF power, while the vibrational temperature remains constant in the studied range of RF powers. Both quantities show no appreciable spatial dependence. The obtained high values of the vibrational temperatures indicate a high population of the vibrational levels, favourable for the volume negative ion production. A theoretical concept indicates the presence of an optimum value for the vibrational temperature at which the negative hydrogen ion yield by volume processes has a maximum. Coincidentally, the measured value is close to this optimum. This indicates that the novel concept can provide certain advantages compared to other sources based on volume production. © 2012 American Institute of Physics. [<http://dx.doi.org/10.1063/1.4769853>]

I. INTRODUCTION

The idea for achieving controlled thermonuclear fusion has stimulated numerous research and development efforts in the past few decades. One such task is the development of an efficient negative hydrogen ion source. The negative ions are needed for the production of high-energy neutral beams for secondary heating of the fusion plasma. In fact, the neutral beam injection (NBI) is foreseen as the main auxiliary heating and current drive system in the international thermonuclear experimental reactor (ITER). As a result, a lot of efforts have been dedicated to the development, optimisation and investigation of the negative hydrogen ion sources.^{1–8} These efforts range from basic studies on the elementary processes governing low-pressure hydrogen discharges^{9,10} (considering also the isotope effects) and probing concepts on small-scale experimental devices^{6,7,11–13} to investigations on real-size devices.^{4,5,11,14} Different discharges and geometries have been developed and tested.^{11,13,15} Finally, the radio-frequency (RF) driven two-chamber plasma source developed at IPP Garching⁵ has been established as a baseline concept for the ITER NBI system. The negative ion production in this source relies on conversion of positive ions and atoms on cesiated surfaces. Different aspects of the source have been targeted in the recent years by both experiments and simulations—basic plasma parameters,^{7,16,17} position and configuration of the magnetic filter field,^{18,19} extraction grid design and extraction voltages,^{4,20} cesium dynamics,^{21,22} long-term operation.^{22,23}

Negative ion sources find also applications for particle accelerators^{24,25} where easy stripping of electrons from ions offers certain advantages for the acceleration and the confinement of the protons in the accelerator. Different types of

sources are used²⁵ but the negative ion production mechanisms are essentially the same—volume-based or surface-based electron attachment. The production of the negative ions on cesiated surfaces—as opposed to the ion production in the volume of the source—shows, in principle, higher negative ion yield at lower pressures required for applications in combination with lower co-extracted electron currents—as is the case for ITER.⁴ However, the use of cesium is associated with some drawbacks and alternatives are desirable. For accelerator applications, the requirements for co-extracted electrons are not so stringent and therefore the existing volume-based sources are widely used. In case of neutral beam sources in fusion applications, however, the available volume-based sources fail to meet these requirements. However, for general applications, there is still a continuing interest in improvement of volume based sources leading to ongoing attempts and investigations in finding better alternatives to surface production. Possibilities are sought for enhancement of the negative ion production in the volume. A promising concept is offered by the matrix source.²⁶ It relies solely on volume production of the negative ions by dissociative electron attachment to vibrationally excited hydrogen molecules. Due to the drift in the ambipolar field, the negative ions are bunched in the center of the discharge.⁷ It was shown that the amount of negative ions in the on-axis region correlates with the radius of the discharge tube.²⁷ The concept is then to stack many small-radius discharges in a matrix configuration.

The source studied here seeks to investigate another possibility for a cesium-free production of negative ions. The source is designed to enhance the volume production mechanism of negative hydrogen ions through optimization of the production of vibrationally excited molecules $H_2(v)$. By providing suitable conditions for atom recombination on the walls, known to play an important role in the hydrogen atom

^{a)}E-mail: Tsanko.Tsankov@rub.de.

balance at low pressures,²⁸ it is thought to be possible to increase the overall population of vibrationally excited molecules in the discharge and therefore to enhance the negative ion production in the volume. The source is with an external magnetic field in an X-point configuration which is an additional element, intended to enhance the overall performance of the source.²⁹ Its role is to separate the power deposition region from the negative ion production zone and to additionally enhance the plasma production at the low pressures required for such sources. It has been already shown³⁰ through the emission from the plasma that the magnetic field configuration influences the distribution of the plasma parameters and under certain conditions also leads to the formation of peculiar structures.³¹

This study is an initial step in the assessment of the feasibility of the proposed concept for negative hydrogen ion production. The population of vibrationally excited molecules—the precursor for volume production of negative ions—is estimated by measuring the vibrational temperature from the Fulcher- α band. Although the vibrational population of the hydrogen molecule ground state could be far from equilibrium, especially in negative hydrogen ion sources,^{8,32,33} a vibrational temperature could still be assigned as a rough measure for the degree of vibrational excitation of the molecules. In this sense, it is a parameter directly connected with the effectiveness of the source concept. It is further shown that an arbitrary high vibrational excitation is actually contra-productive for the negative ions and an optimum value of the vibrational temperature exists. The measured values coincidentally lie close to this optimum. The Fulcher- α band further provides information on the rotational temperature which is considered as indicative for the gas temperature. The gas temperature in turn is important for a number of effects, like, e.g., neutral gas depletion³⁴ and diffusive losses, determining the electron temperature.³⁵

II. EXPERIMENTAL SETUP AND SOURCE CONCEPT

The source is sketched in Figure 1. The plasma chamber consists of a stainless steel vessel with a radius of 22 cm. It supports a quartz top with a diameter of 13 cm and a length of 12 cm. The plasma is sustained by inductively coupling RF power at 13.56 MHz by a flat antenna. The magnetic field configuration is achieved by a dc current flowing in opposite directions in two coils, connected in series. The distance between the inner sides of the coils is 8 cm, the thickness is 4 cm and the plane of the X-point is 4 cm away from the bottom of the quartz top (5 cm from the antenna). The inner radius of the coils amounts to 15 cm.

The experimental results presented in this study are obtained at a hydrogen gas pressure of 1 Pa and a constant gas flow of 5.2 sccm. The power delivered to the plasma (forward minus reflected power as read on the RF generator readout) is varied between 500 and 1000 W. The current creating the static magnetic field is 100 A, resulting in a maximal magnetic field strength of less than 10 mT.

The magnetic field configuration provides efficient separation of the plasma volume into two regions³⁰ marked in Figure 1. The plasma is created in the region close to the RF

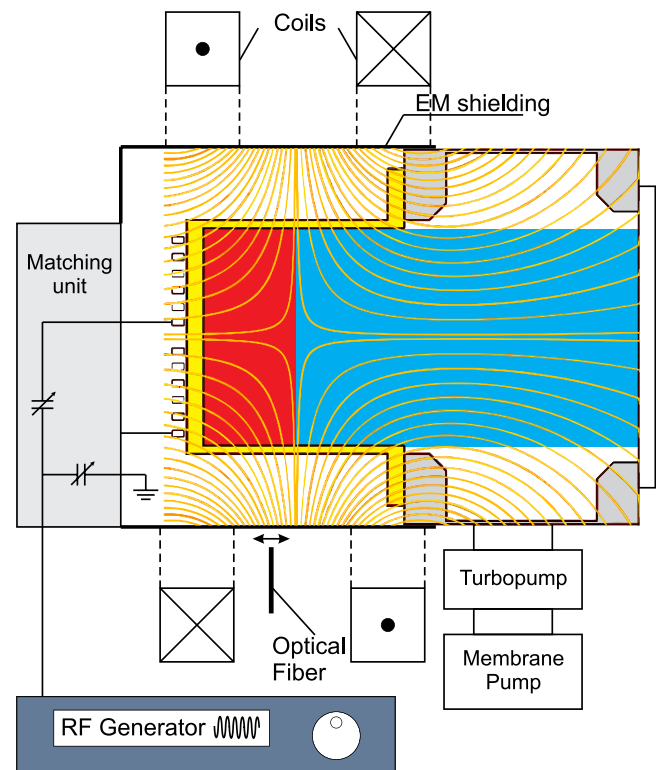


FIG. 1. Schematic presentation of the source. The different regions crucial for the negative ion production are marked by coloured areas: plasma production/molecule dissociation region (red), atom recombination surface (yellow), and negative ion production region (blue). The magnetic field lines are also shown.

antenna. This is also the region, where most of the dissociation of the hydrogen molecules is expected to occur. In the plane of the X-point the magnetic field lines are running purely in radial direction, i.e., perpendicular to the plasma transport direction. This hinders the transport of energy and charged particles from the plasma production zone to the rest of the chamber. The effect is similar to the one of the standard magnetic filters used in the negative ion sources for electron cooling. Therefore, in the region beyond the X-point plane (as seen from the RF antenna), the main source of energy for the electrons are the excited neutral species and the electron temperature is much lower than in the plasma production region. In this sense, this region resembles an afterglow. This is also the region where the extraction of the negative ions should be located.

The hydrogen atoms, resulting from the dissociation in the region close to the RF antenna, can then reach the walls of the quartz top. Some of the atoms can stick to the walls and others can combine with the atoms already on the surface to form hydrogen molecules. Due to the difference of the binding energy of the atoms to the walls and the dissociation energy of the hydrogen molecule, the resulting molecules can be in a vibrationally excited state. It has to be noted that the distribution of vibrational levels, resulting from this mechanism could be quite different from the one, obtained by electron impact excitation. Furthermore, by varying the wall material and, hence, the surface binding energy and sticking probabilities, it might be even possible to influence this vibrational distribution.

The magnetic field lines in the region beyond the X-point are mostly parallel to the plasma flow direction (Figure 1). Therefore, no drifts are expected to occur. Moreover, the whole magnetic field and plasma configuration are axisymmetric, leading to azimuthal homogeneity, as is also observed by the optical emission from the plasma.³⁰ At the present stage as a disadvantage of this configuration could be pointed out the lack of a mechanism for the suppression of the co-extracted electrons. This would certainly be a problem for the application of the setup as real source of negative ions and needs to be addressed on a later stage of the development. However, the current emphasis lies solely on the feasibility of the concept.

For the collection of the plasma light, an optical fiber with a numerical aperture of 0.22 and movable in axial direction between the two coils for the magnetic field is used. The solid angle of the fiber is limited to provide an axial extension of the region of light collection in the far end of the chamber that is smaller than 1 cm. In this way, an on-axis spatial resolution better than 1 cm is ensured. The light is fed to a 2 m spectrograph and registered by a CCD camera (Princeton Instruments, IVUV-700).

The temperatures are deduced from the intensity distribution in the first four vibrational diagonal transitions of the Fulcher- α band. In each vibrational band, the first five rotational lines (Q1–Q5) originating from the rotational levels with $J = 1–5$ are visible and well distinguishable (Figure 2) and hence are used in the data processing. The Fulcher- α band originates from a transition between two triplet states of the hydrogen molecule $d^3\Pi_u \rightarrow a^3\Sigma_g^+$ (Figure 3). The upper state of the transition ($d^3\Pi_u$) is excited by direct electron impact from the ground molecular state ($X^1\Sigma_g^+$). Assuming a Franck-Condon type of excitation, the vibrational and rotational populations of the ground state are mapped onto the upper state. At higher pressures due to collisions the rovibrational distribution of the upper state can relax to an equilibrium distribution and the information about the distribution in the ground state is lost. At lower pressures,

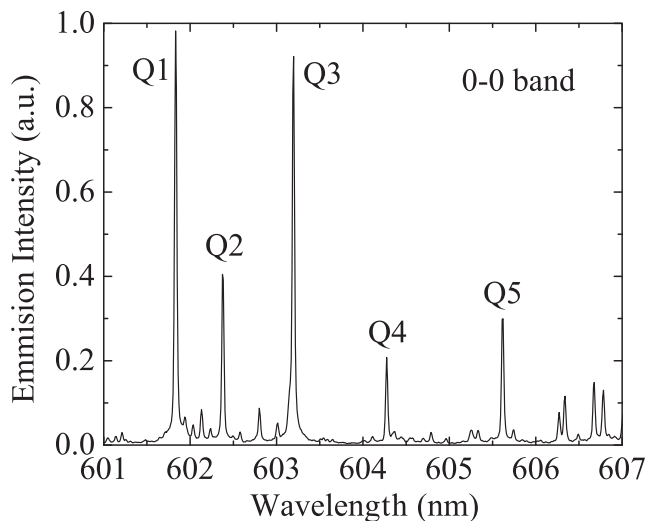


FIG. 2. Typical recorded spectrum for the first diagonal band (0-0) of the Fulcher- α series. The different rotational lines are marked. The plasma conditions are 1 Pa and 1 kW, axial position 2 cm below the quartz.

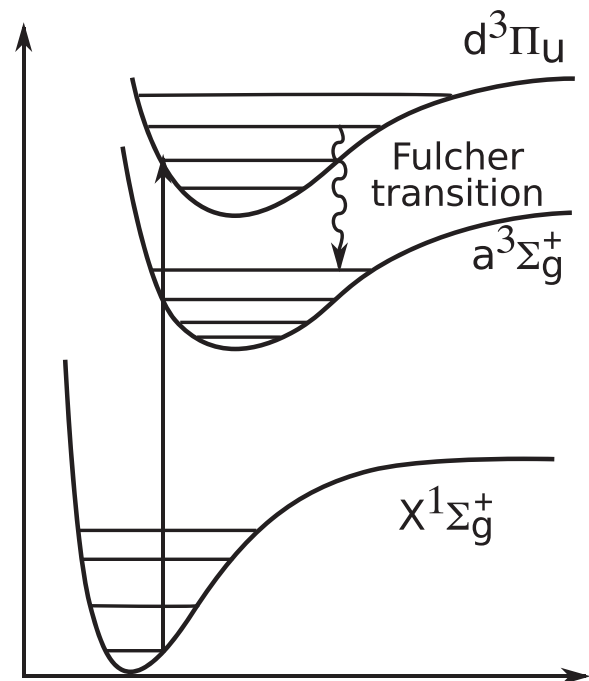


FIG. 3. Schematic representation of the energy levels of the hydrogen molecule, associated with the Fulcher- α band emission. The ground state ($X^1\Sigma_g^+$) is also shown.

the times between the collisions are long enough to allow the upper state to radiate before reaching equilibrium. In this case, the distribution of the emission intensity in the band contains information about the rovibrational distribution of the ground state. The estimations show that under the conditions of the experiment here the low pressure case is fulfilled, therefore, justifying the use of the intensity for measuring the distributions of the ground state.

III. RESULTS AND DISCUSSION

A. Gas temperature

A Boltzmann plot of the intensity distribution of the rotational lines provides information about the rotational temperature of the upper emitting state ($d^3\Pi_u$). As already mentioned, at higher pressures, this state is in equilibrium with the neutral gas and it can be assumed that this rotational temperature is representative for the gas temperature.³⁶ In the low pressure case, valid for the experimental conditions studied here, the rotational population of the $d^3\Pi_u$ level is not in equilibrium with the thermal motion of the gas but instead maps the population of the molecule ground electronic state ($X^1\Sigma_g^+$). In this case, the rotational temperatures of the ground (T_{rot}^X) and the upper (T_{rot}^d) state are connected through the ratio of the rotational constants of the two states:³⁷ $T_{rot}^X/T_{rot}^d = B^X/B^d$. The rotational constants are³⁸ $B^X = 60.809 \text{ cm}^{-1}$ and $B^d = 30.364 \text{ cm}^{-1}$. Furthermore, it can be reasonably assumed that the rotational distribution of the ground state is in equilibrium with the gas, i.e., the rotational temperature of the ground state is equal to the gas temperature $T_{rot}^X = T_{gas}$. Finally, the gas temperature is estimated as approximately twice the inferred rotational temperature: $T_{gas} \approx 2T_{rot}^d$.

The intensity of the Q(2-2) branch of the Fulcher- α band is commonly used for the determination of the gas temperature.³⁶ However, here the rotational and the corresponding gas temperature are obtained separately from each of the measured vibrational bands in the spectrum. Figure 4 shows a typical example for the case of 1 kW absorbed power and a pressure of 1 Pa. It is seen that the temperatures obtained from the first three bands agree well within the experimental uncertainties, while the temperatures resulting from the Q(3-3) band are always somewhat lower. The discrepancy is suspected to be caused by deviations from the Boltzmann distribution of the level population in this particular band, most likely due to predissociation. However, the investigation of the exact reason is beyond the scope of this work. In the following, the average of the results from the first three bands is taken as the gas temperature.

Figure 5 shows the results for the gas temperature obtained at different powers and at different positions in the discharge. It is seen that the temperature increases with the power. Actually, the increase of the spatially averaged gas temperature with the power is linear. This is not surprising, since with the power increase, the plasma density also increases. This leads to more frequent collisions between the electrons and the gas molecules and therefore to a larger energy transfer from the electrons to the neutral gas. The charged particle fluxes to the walls also increase, leading to an increase of the energy deposited there. Therefore, the increase in the power leads also to an increase in the temperature of the walls. Due to the low pressure, the walls are in a good thermal contact with the neutral gas and, hence, the increase of the wall temperature with the power is another reason for the increase in the gas temperature.

The almost negligible decline of the temperature with the distance from the antenna—most pronounced at 1 kW—is attributed to the spatial distribution of the plasma density on one side and to variation of the wall temperature on the other. The magnetic field configuration results in a higher

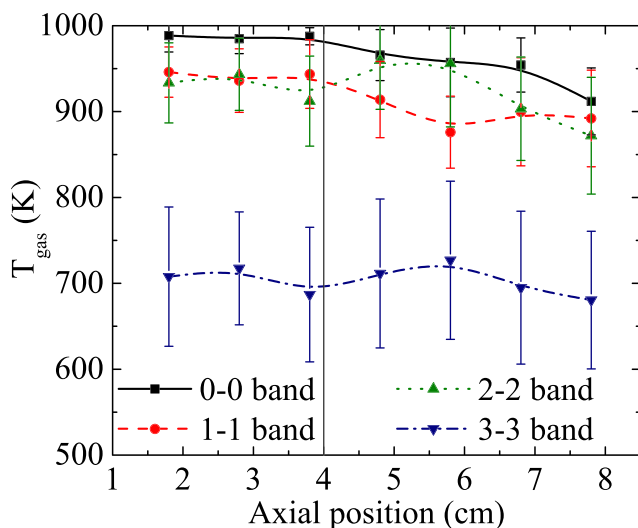


FIG. 4. The gas temperature obtained from the spectrum corresponding to the different vibrational bands at 1 Pa and 1 kW. The antenna producing the discharge is at an axial position of -1 cm and the vertical line indicates the position of the X-point plane.

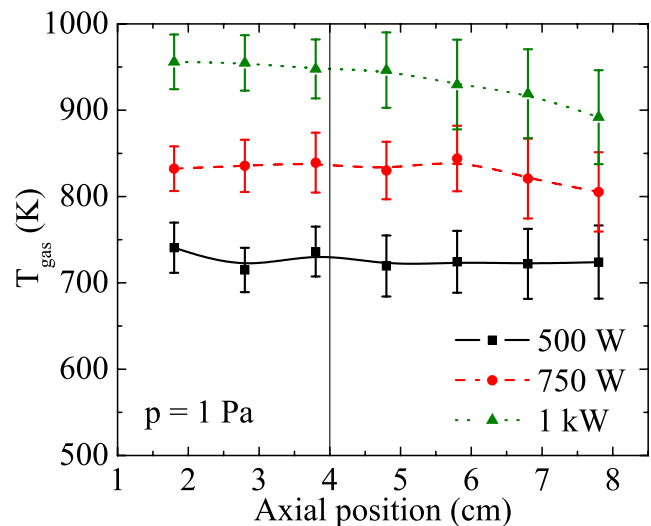


FIG. 5. Gas temperatures obtained at different powers and a pressure of 1 Pa. The antenna producing the discharge is at an axial position of -1 cm and the vertical line indicates the position of the X-point plane.

plasma density in the region close to the RF antenna. This is confirmed by the visible emission intensity distribution.³⁰ The higher plasma density favours higher energy transfer to the gas both by elastic collisions with electrons and by collisions with energetic ions and atoms, which are expected to be abundant close to the antenna. Furthermore, more energy is being delivered in this region also to the walls. Due to the low heat conductivity of the wall materials (quartz and stainless steel), gradients of the wall temperature exist. As a result, the wall temperature is highest in the region close to the antenna and decreases towards the metal chamber. These effects are more pronounced at higher RF power levels. This could explain the spatial gradients in the gas temperature observed at higher powers and practically absent at the lower power studied here.

Furthermore, the inflow of colder gas downstream could also play a certain role. In any case, one should note that the obtained spatial variations in the temperature are within the experimental uncertainties. This allows one to assume a homogeneous gas temperature in the source. Therefore, the presence of the X-point seems to play negligible to no role for the spatial distribution of the gas temperature.

B. Vibrational temperature

The vibrational temperature T_{vib} is obtained from the intensity distribution in the vibrational bands. The notion of vibrational “temperature” deserves some special consideration. It has been shown that the vibrational distribution function (VDF) in negative hydrogen ion sources can significantly deviate from equilibrium, in particular, at higher vibrational states ($v \geq 6$).^{8,32,33} This is due to the different mechanisms leading to the excitation of the lower and upper vibrational states. The lower ones ($v < 6$) are primarily excited by electron impacts from the ground vibrational state ($v=0$). The upper levels ($v > 6$) are populated by electron impact excitation of higher electronic molecular states (mainly the $B^1\Sigma_u^+$ state), followed by a radiative decay to the

ground state. Since the potential curves of the excited electronic states are shifted with respect to the one of the ground state, the radiative decay leads to preferential population of the higher vibrational states.

In the source under study here, the wall formation mechanism of hydrogen molecules could further lead to deviations from the equilibrium Boltzmann distribution of the vibrational states. The different mechanisms of atom recombination—Langmuir–Hinshelwood or Eley–Rideal—are expected to produce similar distributions,³⁹ however, some differences exist. For example, in the case of the Langmuir–Hinshelwood mechanism the two recombining atoms are first adsorbed on the surface and then diffuse to each other. It is then expected that the resulting molecules are in thermal equilibrium with the walls³⁹ and the wall temperature could therefore play a significant role in determining the population of vibrational states. The energy released from the binding of the two atoms in a molecule is used to release both atoms from the surface. The remaining energy (3.9 eV in this case⁴⁰) is shared by the surface and the molecule, thus, allowing the formation of molecules with a vibrational number v up to 10. In the other case of the Eley–Rideal mechanism, an incoming atom collides and recombines directly with an adsorbed atom on the surface. In this situation the wall temperature is of less significance.³⁹ Furthermore, the energy from the molecule formation is used to release only one adsorbed atom and the available energy for molecule excitation is slightly larger⁴⁰ (4.1 eV). This mechanism of atom recombination can then produce molecules with v up to 11. According to Kim and Boudart,⁴¹ on a flat atomic level surface, the binding energy of the atom is even lower, which would allow even molecules with $v = 12$ to be produced. It is however hard to predict the final vibrational distribution of the molecules in the discharge and at the current stage it is not possible to give a more specific quantitative description.

In any case, strictly speaking, the term “temperature” cannot be used. Here, it is used merely as a parameter, describing the relative population of the vibrationally excited states and inferred by least squares fitting. It cannot in any way give their absolute number density. If the shape of the VDF is a known analytic function, described by a few parameters, these could be in principle also obtained by a minimization procedure. However, since the shape of the VDF is not known for the source under study, more rigorous determination of the vibrational populations is not possible at this time.

It is further assumed that the sum of the intensities of the first five observed rotational transitions give the net intensity of the vibrational band. Some authors assume that even the sum of the first two strongest rotational lines (Q1 and Q3 for H₂) already give a good representation of the integrated vibrational spectrum.⁴² Assuming further a Boltzmann distribution of the vibrational levels n_v of the ground $X^1\Sigma_g^+$ state and population of the upper $d^3\Sigma_u$ state according to the Franck-Condon principle results in the following expression for the population density of the upper states $N_{v'}$:

$$N_{v'} = \sum_{v=0}^{14} q_{v'v} n_v \propto \sum_{v=0}^{14} q_{v'v} \exp\left(-\frac{E_v}{kT_{\text{vib}}}\right). \quad (1)$$

Here $q_{v'v}$ are the Franck-Condon factors taken from Ref. 10 and E_v are the ground state vibrational energies. The vibrational temperature is then obtained from minimization of the expression:

$$\chi^2 = \sum_{v'=1}^3 \left(\frac{A_{v'} N_{v'}}{A_0 N_0} - \frac{I_{v'}}{I_0} \right)^2, \quad (2)$$

where $I_{v'}$ are the measured intensities of the vibrational $v' - v'$ transition and $A_{v'}$ are the transition probabilities of the corresponding upper level taken from Ref. 10. In Eq. (2), the line ratios can be taken not only with respect to the intensity of the 0-0 transition, as is done further on, but also with respect to any of the measured vibrational bands. However, this results always in effectively the same value of the vibrational temperature.

Figure 6 shows the obtained results for the vibrational temperature. The temperature is practically constant in axial direction and, similarly to the gas temperature, does not seem to be influenced by the presence of the X-point. The relatively low gas pressure is certainly the main cause for the homogenization of the vibrational population and of the gas temperature. This means that regardless of the spatial position of the molecule vibrational excitation region, the excited molecules fill the entire chamber of the source. This fact is beneficial for the production of the negative ions but does not allow a clear conclusion on the exact mechanism responsible for the molecule vibrational excitation to be drawn.

A notable difference from the gas temperature is that the vibrational temperature exhibits no significant dependence on the power variation in the investigated range of powers. This indicates that the vibrational population is rather independent on plasma density which would be in agreement with the concept of surface production of vibrational excited molecules. To draw a conclusion, further investigations are necessary.

It has to be noted that the Franck-Condon matrix $q_{v'v}$ shows that the measured intensities, corresponding to

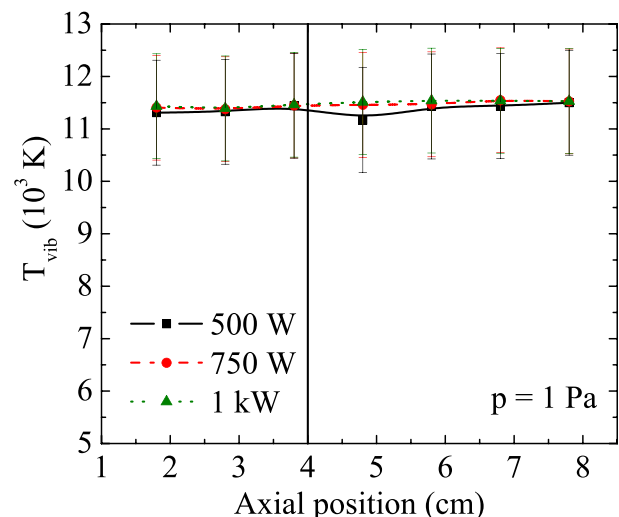


FIG. 6. Vibrational temperatures obtained at different powers and a pressure of 1 Pa. The antenna producing the discharge is at an axial position of -1 cm and the vertical line indicates the position of the X-point plane.

$v' = 0 - 3$, are most sensitive to the lower vibrational levels with v up to 7. Therefore, it should be further emphasized that the measurement results represent better the lower part of the vibrational population of the ground state than the higher. Furthermore, due to the low difference in energy between the vibrational levels as compared to the obtained values of the vibrational temperature, the method becomes less sensitive to changes in the vibrational temperature.⁴³ This results in rather high uncertainty of about 1000 K.

C. Effect on the negative hydrogen ion density

The results in the previous subsection reveal the relatively high degree of vibrational excitation of the hydrogen molecules established in the source. These can undergo superelastic collisions with the electrons and heat them, leading to an enhancement of the stripping losses through electron collisions with the negative ions. Therefore, one could conclude, that a higher degree of vibrational excitation is not necessarily beneficial for the volume-based sources. This is in contrast to what is usually sought in some investigations.⁴⁴

To better explain the effect of the vibrational temperature on the negative ion population, a simplistic estimation can be made. It is based on the fact that in the afterglow of a hydrogen discharge, the electron energy is coupled by super-elastic collisions to the vibrationally excited molecules.⁴⁵ The region of negative ion formation in tandem sources has certain similarities to an afterglow of a pulsed plasma and a similar behaviour is to be expected. Both situations are characterized with negligible external heating of the electrons and the plasma is sustained by the energy stored in the heavy particles. Therefore, following the kinetic concept developed in Ref. 45, the effect of the super-elastic collisions is to map the electron energy distribution function (EEDF) $f(\varepsilon)$ to higher energies

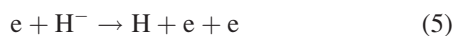
$$f(\varepsilon + \Delta E) = \alpha f(\varepsilon). \quad (3)$$

Here $\Delta E = E_1 - E_0$ is the energy spacing between the $v = 1$ and $v = 0$ vibrational states of the ground electronic state of the hydrogen molecule and $\alpha = \exp(-\Delta E/kT_{\text{vib}})$ is the ratio of the densities of these states. Assuming a Maxwellian EEDF with an electron temperature T_e , Eq. (3) imposes that $T_e = T_{\text{vib}}$, i.e., thermal equilibrium is established.

In volume based negative hydrogen ion sources, the main production mechanism of H^- is by dissociative attachment (DA) to vibrationally excited molecules $\text{H}_2(v)$



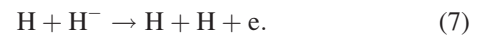
This process is described by a rate constant $k_{DA}(v)$ for DA from each individual vibrational level. The destruction processes are due to electron impact detachment (with a rate k_{Det})



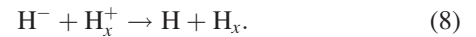
and associative



and non-associative detachment



The last two reactions are described with a combined rate k_H . When the negative ion density is high enough, a further loss channel for the ions is the mutual neutralization with positive ions (with a rate constant k_{rec})



Since the rate constants for the recombination with the different types of positive ions have equal values,⁴⁶ the dominating type of positive ions are not of significance for the final result.

The temperature of the negative ions is usually lower than the electron temperature. The negative ions are then confined in the potential well of the ambipolar field and the diffusion has almost no contribution to the losses of negative ions.⁷ The negative ion density is then determined by the following rate equation:

$$\sum_{v=0}^{14} k_{DA}(v)n_v n_e = k_{Det}n_e n_- + k_{rec}n_+ n_- + k_H n_a n_-. \quad (9)$$

Here n_e and n_a are the densities of the electrons and of the hydrogen atoms, respectively. The density of the positive ions n_+ is given by the quasineutrality condition $n_+ = n_e + n_-$. From Eq. (9), the negative ion density n_- is obtained

$$n_- = \frac{k_{Det}n_e + k_{rec}n_e + k_H n_a}{2k_{rec}} \times \left[-1 + \sqrt{1 + \frac{4k_{rec}n_e \sum_{v=0}^{14} n_v k_{DA}(v)}{(k_{Det}n_e + k_{rec}n_e + k_H n_a)^2}} \right]. \quad (10)$$

For the calculation, the cross-sections are taken from Ref. 9 and integrated with a Maxwellian EEDF with $T_e = T_{\text{vib}}$ for $k_{DA}(v)$ and k_{Det} . For k_H , a Maxwellian distribution in the center of mass system with relative temperature $T = T_{\text{gas}} = 800$ K is used (Figure 5). Since the dissociation of the hydrogen molecule proceeds through the repulsive $b^3\Sigma_u^+$ state, the atoms can have an energy higher than the mean thermal energy—the so-called Franck-Condon energy. However, the energy of the hydrogen atoms does not influence the dependence of the negative ion density on the vibrational temperature, only their absolute density is reduced, when the atom temperature is increased. Further, for the calculation, an electron density of $5 \times 10^{16} \text{ m}^{-3}$ is assumed. The hydrogen atoms density is obtained by assuming that their density constitutes 5% of the molecule density and keeping the sum of both constant. These values are rough estimates, but are consistent with a global power and density estimations.

It has to be further noted that the production term in Eq. (10) is probably underestimated due to expected deviations at higher vibrational levels from the Boltzmann distribution. However, the energy spacing between the levels decreases

with v . Therefore, an overpopulation of the higher-lying levels is not expected to considerably influence the electron temperature, and hence, the stripping losses (5). Consequently, the dependence of n_- on T_{vib} should not be significantly affected by it.

The resulting negative ion density as a function of the vibrational temperature is depicted in Figure 7. The increase of the density with the vibrational temperature in the region $T_{\text{vib}} \leq 1$ eV is the standard results, usually discussed in the literature. However, the decrease at higher values of the vibrational temperature is a direct consequence of the coupling of the vibrational excitation and the electron energy, leading to higher destruction rates by electron impact. This leads to the formation of a maximum for a vibrational temperature between 1 and 1.5 eV. Noteworthy, the measured values lie close to this interval.

The behavior of the negative ion density with the vibrational temperature is further illustrated in Figure 8, where the destruction terms of H^- are directly compared. At lower vibrational temperatures, the negative ions are predominantly destroyed by collisions with the atoms and by recombination with the positive ions. At higher temperatures, the electron impact collisions start to dominate. Since the ratio of the atom to molecule density is kept constant, the destruction rate by atomic collisions is independent from the value of the vibrational temperature. In reality, however, higher densities of the excited molecules would lead to higher dissociation degrees. This will act twofold in the direction of reducing the negative ion density: on one side, the destruction rate by atomic collisions will increase and on the other the total number density of the hydrogen molecules will decrease.

In summary, the above discussion shows that there should exist an optimum value of the vibrational temperature at which the density of the volume produced negative hydrogen ions attains a maximum. This topic should be further investigated to better understand the boundaries imposed by this effect on the possibility for volume production of negative ions.

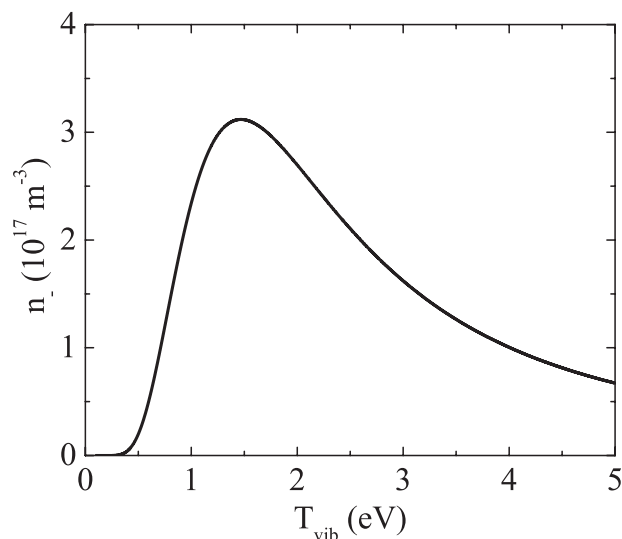


FIG. 7. Estimated negative hydrogen ion density.

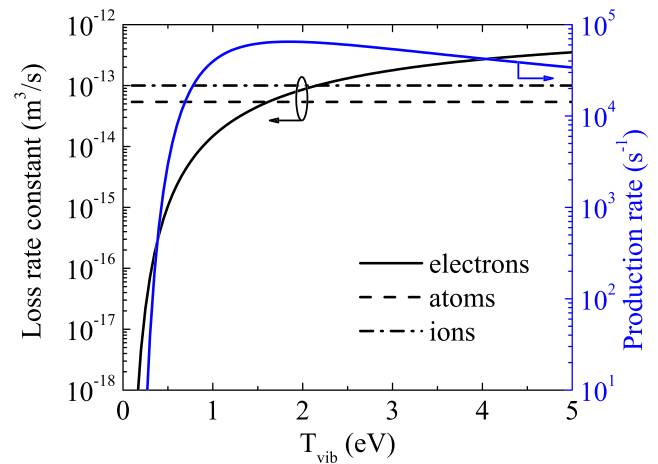


FIG. 8. Comparison of the H^- -destruction rate by electron impact, by collisions with the atoms and by recombination with the positive ions. The variation of the production rate is also given.

IV. CONCLUSIONS

The spatially resolved emission intensity of the Fulcher- α band has been recorded at various conditions in a source developed for negative hydrogen ion production. The aim of this source is to assess the feasibility of a concept for production of negative ions by dissociative attachment in the volume from vibrationally excited molecules produced on the surface. As a first step in the investigation, an analysis of the emission is made, yielding the rotational and vibrational temperatures in the source. The gas temperature is assumed to be identical to the rotational temperature of the ground state. Both the gas and the vibrational temperatures show no appreciable spatial variation. However, while the gas temperature increases with power, the vibrational one remains almost constant with a value close to 1 eV.

This high degree of vibrational excitation raises the question for the influence of the vibrational temperature on the negative hydrogen ion density. The analysis shows that there should exist an optimal value for the vibrational temperature. Coincidentally, the measured value agrees well with this optimum. This indicates that the novel source concept introduced here can provide certain advantages compared to other negative ion sources based on volume production.

ACKNOWLEDGMENTS

Ts.V.Ts. gratefully acknowledges the support by the Alexander von Humboldt Foundation.

¹M. Bacal, C. Courteille, R. Leroy, and R. Stern, *AIP Conf. Proc.* **287**, 558 (1992).

²M. Bacal, *Plasma Sources Sci. Technol.* **2**, 190 (1993).

³M. Bacal, *Nucl. Fusion* **46**, S250 (2006).

⁴U. Fantz, P. Franzen, W. Kraus, M. Berger, S. Christ-Koch, H. Falter, M. Fröschele, R. Gutser, B. Heinemann, C. Martens, P. McNeely, R. Riedl, E. Speth, A. Stäbler, and D. Wunderlich, *Nucl. Fusion* **49**, 125007 (2009).

⁵A. Staebler, U. Fantz, P. Franzen, M. Berger, S. Christ-Koch, H. D. Falter, M. Fröschele, R. Gutser, B. Heinemann, D. Holtum, W. Kraus, C. Martens, P. McNeely, R. Nocentini, S. Obermayer, R. Riedl, E. Speth, and D. Wunderlich, *Fusion Eng. Des.* **84**, 265 (2009).

- ⁶Zh. Kiss'ovski, St. Kolev, S. Müller, Ts. Paunskaa, A. Shivarova, and Ts. Tsankov, *Plasma Phys. Controlled Fusion* **51**, 015007 (2009).
- ⁷Ts. Paunskaa, A. Shivarova, Kh. Tarnev, and Ts. Tsankov, *Phys. Plasmas* **18**, 023503 (2011).
- ⁸Th. Mosbach, H.-M. Katsch, and H. F. Döbele, *Phys. Rev. Lett.* **85**, 3420 (2000).
- ⁹R. K. Janev, D. Reiter, and U. Samm, "Collision processes in low-temperature hydrogen plasmas," Technical Report No. Jül-4105, Forschungszentrum Jülich.
- ¹⁰U. Fantz and D. Wunderlich, "Franck-Condon factors, transition probabilities and radiative lifetimes for hydrogen molecules and their isotopomers," Technical Report No. INDC(NDS)-457, 2004.
- ¹¹M. Bacal, *Rev. Sci. Instrum.* **71**, 3981 (2000).
- ¹²Zh. Kiss'ovski, St. Kolev, A. Shivarova, and Ts. Tsankov, *IEEE Trans. Plasma Sci.* **35**, 1149 (2007).
- ¹³O. Fukumasa, M. Hosoda, and H. Naitou, *Rev. Sci. Instrum.* **63**, 2696 (1992).
- ¹⁴E. Speth, H. Falter, P. Franzen, B. Heinemann, M. Bandyopadhyay, U. Fantz, W. Kraus, P. McNeely, R. Riedl, A. Tanga, and R. Wilhelm, *Fusion Eng. Des.* **74**, 279 (2005).
- ¹⁵P. Franzen, H. D. Falter, U. Fantz, W. Kraus, M. Berger, S. Christ-Koch, M. Fröschle, R. Gutser, B. Heinemann, S. Hilbert, S. Leyer, C. Martens, P. McNeely, R. Riedl, E. Speth, and D. Wunderlich, *Nucl. Fusion* **47**, 264 (2007).
- ¹⁶M. Berger, U. Fantz, S. Christ-Koch, and NNBI Team, *Plasma Sources Sci. Technol.* **18**, 025004 (2009).
- ¹⁷G. J. M. Hagelaar, G. Fubiani, and J.-P. Boeuf, *Plasma Sources Sci. Technol.* **20**, 015001 (2011).
- ¹⁸I. Djermanov, St. Kolev, St. Lishev, A. Shivarova, and Ts. Tsankov, *J. Phys.: Conf. Ser.* **63**, 012021 (2007).
- ¹⁹St. Kolev, St. Lishev, A. Shivarova, Kh. Tarnev, and R. Wilhelm, *Plasma Phys. Controlled Fusion* **49**, 1349 (2007).
- ²⁰E. Speth, H. Falter, P. Franzen, U. Fantz, M. Bandyopadhyay, S. Christ, A. Encheva, M. Fröschle, D. Holtum, B. Heinemann, W. Kraus, A. Lorenz, C. Martens, P. McNeely, S. Obermayer, R. Riedl, R. Süß, A. Tanga, R. Wilhelm, and D. Wunderlich, *Nucl. Fusion* **46**, S220 (2006).
- ²¹U. Fantz, R. Gutser, and C. Wimmer, *Rev. Sci. Instrum.* **81**, 02B102 (2010).
- ²²U. Fantz and C. Wimmer, *Rev. Sci. Instrum.* **83**, 02B110 (2012).
- ²³W. Kraus, U. Fantz, and P. Franzen, *Rev. Sci. Instrum.* **81**, 02B110 (2010).
- ²⁴G. I. Dimov, *Rev. Sci. Instrum.* **67**, 3393 (1996).
- ²⁵I. S. Hong, Y. S. Hwang, and Y. S. Cho, *Rev. Sci. Instrum.* **73**, 979 (2002).
- ²⁶St. Lishev, Ts. Paunskaa, A. Shivarova, and Kh. Tarnev, *Rev. Sci. Instrum.* **83**, 02A702 (2012).
- ²⁷Ts. Paunskaa, A. Shivarova, and Kh. Tarnev, *J. Appl. Phys.* **107**, 083301 (2010).
- ²⁸I. Koleva, Ts. Paunskaa, H. Schlüter, A. Shivarova, and Kh. Tarnev, *Plasma Sources Sci. Technol.* **12**, 597 (2003).
- ²⁹Ts. Tsankov and U. Czarnetzki, *AIP Conf. Proc.* **1390**, 140 (2011).
- ³⁰Ts. Tsankov and U. Czarnetzki, *IEEE Trans. Plasma Sci.* **39**, 2538 (2011).
- ³¹Y. Celik, Ts. Tsankov, and U. Czarnetzki, *IEEE Trans. Plasma Sci.* **39**, 2466 (2011).
- ³²M. Capitelli, O. De Pascale, P. Diomedea, A. Gicquel, C. Gorse, K. Hassouni, S. Longo, and D. Pagano, *AIP Conf. Proc.* **763**, 66 (2005).
- ³³Th. Mosbach, V. Schulz-von der Gathen, and H. F. Döbele, *Contrib. Plasma Phys.* **42**, 650 (2002).
- ³⁴D. O'Connell, T. Gans, D. L. Crintea, U. Czarnetzki, and N. Sadeghi, *J. Phys. D: Appl. Phys.* **41**, 035208 (2008).
- ³⁵Y. Celik, M. Aramaki, D. Luggenhölscher, and U. Czarnetzki, *Plasma Sources Sci. Technol.* **20**, 015022 (2011).
- ³⁶M. Osiac, B. P. Lavrov, and J. Röpcke, *J. Quant. Spectrosc. Radiat. Transf.* **74**, 471 (2002).
- ³⁷S. Iordanova, *J. Phys.: Conf. Ser.* **113**, 012005 (2008).
- ³⁸S. Iordanova, I. Koleva, and Ts. Paunskaa, *Spectrosc. Lett.* **44**, 8 (2011).
- ³⁹M. Cacciatore and M. Rutigliano, *Plasma Sources Sci. Technol.* **18**, 023002 (2009).
- ⁴⁰J. Amorim, J. Loureiro, and D. Schram, *Chem. Phys. Lett.* **346**, 443 (2001).
- ⁴¹Y. C. Kim and M. Boudart, *Langmuir* **7**, 2999 (1991).
- ⁴²U. Fantz and B. Heger, *Plasma Phys. Controlled Fusion* **40**, 2023 (1998).
- ⁴³W. G. Wang, Y. Xu, X. F. Yang, A. M. Zhu, Z. W. Liu, and X. Liu, *Eur. Phys. J. D* **46**, 103 (2008).
- ⁴⁴St. Lishev, A. Shivarova, and Ts. Tsankov, *J. Phys.: Conf. Ser.* **223**, 012001 (2010).
- ⁴⁵M. Osiac, T. Schwarz-Selinger, D. O'Connell, B. Heil, Z. L. Petrović, M. M. Turner, T. Gans, and U. Czarnetzki, *Plasma Sources Sci. Technol.* **16**, 355 (2007).
- ⁴⁶Ts. Paunskaa, H. Schlüter, A. Shivarova, and Kh. Tarnev, *Phys. Plasmas* **13**, 023504 (2006).